



# Interaction of organoruthenium(II)-polypyridyl complexes with DNA and BSA

Aleksandra Margetić · Stefan Nikolić ·  
Sanja Grgurić-Šipka · Miroslava T. Vujčić

Received: 17 January 2022 / Accepted: 26 May 2022  
© The Author(s), under exclusive licence to Springer Nature B.V. 2022

**Abstract** The interaction of four arene ruthenium complexes  $[(\eta^6\text{-}p\text{-cymene})\text{Ru}(\text{Me}_2\text{dppz})\text{Cl}]\text{PF}_6$  (**1**) with  $\text{Me}_2\text{dppz} = 11,12\text{-dimethyldipyrido}[3,2\text{-}a:2',3'\text{-}c]$  phenazine,  $[(\eta^6\text{-}p\text{-cymene})\text{Ru}(\text{aip})\text{Cl}]\text{PF}_6$  (**2**) with  $\text{aip} = 2\text{-}(9\text{-anthryl})\text{-}1H\text{-imidazo}[4,5\text{-}f][1,10]$  phenanthroline),  $[(\eta^6\text{-}toluene)\text{Ru}(\text{ppf})\text{Cl}]\text{PF}_6$  (**3**) and  $[(\eta^6\text{-}p\text{-cymene})\text{Ru}(\text{ppf})\text{Cl}]\text{PF}_6$  (**4**) with  $\text{ppf} = \text{pyrido}[2',3':5,6]$  pyrazino[2,3-*f*][1,10]phenanthroline with calf thymus DNA were investigated. All of four complexes exhibit DNA-binding activity. UV–Vis spectroscopic studies revealed the intrinsic binding constants of the order  $10^4 \text{ M}^{-1}$  of magnitude, indicating non-intercalative mode. Fluorescence quenching analysis showed that all complexes interfere with intercalator ethidium bromide and minor groove binder Hoechst 33258 by a singular non-intercalative mode with extent that differs by two orders of magnitude. Gel electrophoresis results on

DNA cleavage assay demonstrated that all complexes produced conformational changes of supercoiled circular plasmid pUC19 in concentration dependent way. The results of fluorescence titration bovine serum albumin by **1**, **2**, **3** and **4** showed that all complexes significantly quench tryptophan residues fluorescence through a static quenching mechanism. The antimicrobial activity against both Gram-positive and Gram-negative bacteria analyzed. Complex **1** was most active, even on *Escherichia coli* was more active than positive control compound.

**Keywords** Ruthenium(II)-arene complexes · DNA binding study · DNA cleavage experiments · Antimicrobial activity

## Introduction

Cisplatin is widely used to treat testicular, ovarian, head, neck, and small cell lung tumors (Go and Adjei 1999). The activity of this anticancer drug is based on DNA modification (Mantri et al. 2007). Although cisplatin is one of the most used and successful anticancer drug, approved by FDA in 1978, (Sherman and Lippard 1987), due to severe side effects and natural and acquired resistance of patients toward the drug (Kelland 2007) researchers are forced to find better candidates. Among the many metals investigated for this purpose, ruthenium complexes have shown great potential (Lee et al. 2020). For example, NAMI-A

A. Margetić · M. T. Vujčić  
Department of Chemistry, University of Belgrade –  
Institute of Chemistry, Technology and Metallurgy –  
National Institute of the Republic of Serbia, Njegoševa 12,  
11000 Belgrade, Serbia

S. Nikolić  
Innovative Centre Faculty of Chemistry Belgrade,  
University of Belgrade, Studentski trg 12-16,  
11000 Belgrade, Serbia

S. Grgurić-Šipka (✉)  
Faculty of Chemistry, University of Belgrade, Studentski  
trg 12-16, 11000 Belgrade, Serbia  
e-mail: sanjag@chem.bg.ac.rs

and KP1019/1339 showed great potential and entered clinical trials (Alessio and Messori 2019). Ruthenium complexes display multidisciplinary applications, as they can be used in diagnosis (Lin et al. 2018), or as a photosensitizer in photodynamic therapy (Mari et al. 2015). DNA is the main target of most metallo-drugs but the interaction of metallo-drugs with molecular targets other than DNA (Timerbaev et al. 2006) such as serum proteins is important to better understand the mechanism of action because serum albumin performs the transport, distribution, accumulation and excretion properties of drugs in the organism (Ascone et al. 2008). This approach can be used to design a drug that regulates the activities of disease-related proteins such as enzymes or receptors. An active small molecule that binds to the active site of the disease-related proteins with high selectivity and affinity may affect a cure (Lee and Suh 2009) if the unknown active site of protein activates its cleavage (Suh and Chei 2008). Ruthenium(II) polypyridyl complexes are proved to have significant biological properties (Notaro and Gasser 2017). Most complexes are very reactive, imaging capabilities, with binding ability, and kinetically inert at the same time which rank them as potential diagnostic and therapeutic drugs. *N,N*-chelating ligands and octahedral structures allow them to go through the organism to target points. Complexes interact with biological molecules including DNA, proteins and RNA, both as probes and inhibitors. Interaction with these biological molecules often induces damage or toxicity (Zeng et al. 2017).

All kinds of bacterial and other microbial infectious diseases are well-known problems in human history. Pneumonia, also caused by bacteria infection, has four million deaths reported every year (Ruuskanen et al. 2011). Each year, more than 400,000 people die of malaria, with 229 million new malaria infections in 2019 (WHO site, World Malaria Report 2020). Due to the applications of many antimicrobials worldwide, drug-resistant populations of microorganisms emerged. A call for the development of new antimicrobial agents is great. Drugs based upon analogs of known scaffolds proved to be inadequate, due to the possible resistance. A better solution is the development of new classes of antimicrobials, with less potential of resistance occurrence. Ruthenium complexes as well as organoruthenium complexes showed great potential as promising antimicrobial agents (Fangfei et al. 2015).

In our earlier studies, we have investigated cytotoxic activity, drug-accumulation study and fluorescent microscopy of arene ruthenium complexes with intercalating ligands (Nikolić et al. 2016; Pavlović et al. 2019). In this work, four arene ruthenium complexes  $[(\eta^6\text{-}p\text{-cymene})\text{Ru}(\text{Me}_2\text{dppz})\text{Cl}]\text{PF}_6$  (**1**) with  $\text{Me}_2\text{dppz} = 11,12\text{-dimethyldipyrido}[3,2\text{-}a:2',3'\text{-}c]\text{phenazine}$ ,  $[(\eta^6\text{-}p\text{-cymene})\text{Ru}(\text{aip})\text{Cl}]\text{PF}_6$  (**2**) with  $\text{aip} = 2\text{-}(9\text{-anthryl})\text{-}1H\text{-imidazo}[4,5\text{-}f][1,10]\text{phenanthroline}$ ,  $[(\eta^6\text{-}toluene)\text{Ru}(\text{ppf})\text{Cl}]\text{PF}_6$  (**3**) and  $[(\eta^6\text{-}p\text{-cymene})\text{Ru}(\text{ppf})\text{Cl}]\text{PF}_6$  (**4**) with  $\text{ppf} = \text{pyrido}[2',3':5,6]\text{pyrazino}[2,3\text{-}f][1,10]\text{phenanthroline}$  we have embarked on further experiments with the best candidates to interactions with calf thymus DNA (CT-DNA) and bovine serum albumin (BSA), as well as examine antimicrobial properties.

## Experimental

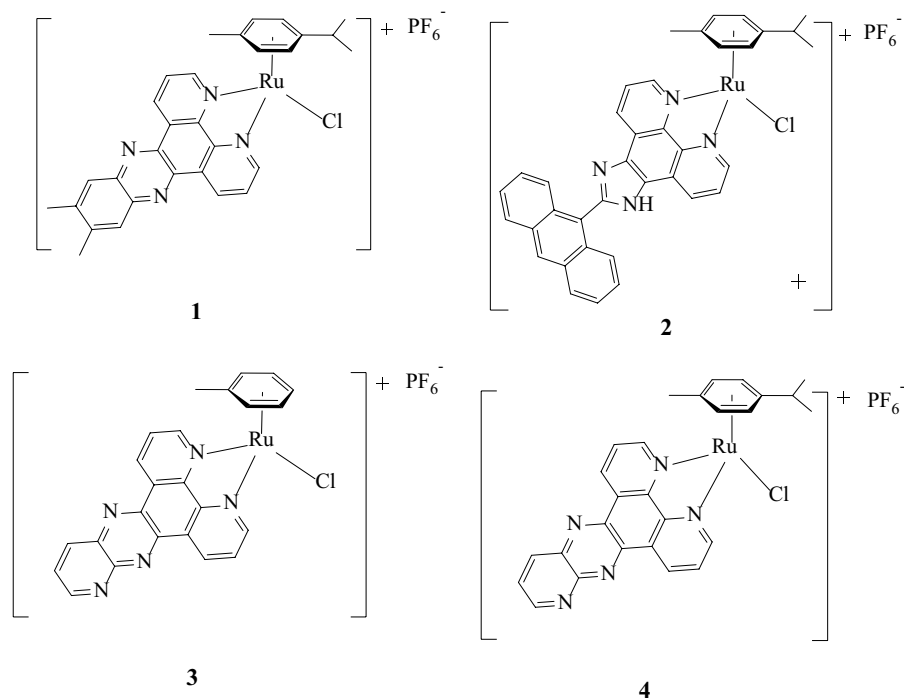
### Chemicals and reagents

All standard chemicals, as well as CT-DNA, BSA, ethidium bromide, Hoechst 33258, Mueller–Hinton broth, were of analytical grade (or higher) and were purchased from Merck (Darmstadt, Germany) or associated companies. Solvents were used as received or dried over molecular sieves.  $\text{RuCl}_3$  was purchased from I2CNS. Complexes **1**, **2**, **3** and **4** were synthesized according to published procedures from Nikolić et al. (2016), Pavlović et al. (2019) (Scheme 1).

### Spectroscopic studies

#### *UV–Vis measurements experiments*

For DNA binding experiments, a calf thymus DNA (lyophilized, highly polymerized, obtained from Serva, Heidelberg) (CT-DNA) was dissolved in bicarbonate buffer (40 mM, pH 8.4) overnight at 4 °C. This stock solution was stored at 4 °C and was stable for several days. A solution of CT-DNA in buffer gave a ratio of UV absorbance at 260 and 280 nm,  $A_{260}/A_{280}$  of 1.89–2.01, indicating that DNA was sufficiently free of protein. The concentration of DNA (3.15 mg/mL) was determined from the UV absorbance at 260 nm using the extinction coefficient  $\epsilon_{260} = 6600 \text{ M}^{-1} \text{ cm}^{-1}$  (Reichmann et al. 1954). All compounds (**1**, **2**, **3** and **4**) were dissolved before use

**Scheme 1** Structures of the complexes **1**, **2**, **3** and **4**

in dimethyl sulfoxide in concentrations of 10 mM and these solutions were used as stock solutions. UV–Vis spectra were recorded on a UV-1800 Shimadzu UV/Visible spectrophotometer operating from 200 to 800 nm in 1.0 cm quartz cells. Spectra of the complexes of the same concentrations were also recorded, as well as spectra of CT-DNA before and after an interaction. Stability and solubility of the complexes was assessed by recording UV–Vis spectra of sample solutions in the bicarbonate buffer during time in applied concentration range. Reaction mixtures (1 mL in 40 mM bicarbonate buffer, pH 8.4) consisting of the complexes and CT-DNA were incubated at 37 °C for 60 min with occasional vortexing. The absorbance titrations were performed at 3  $\mu$ M concentration of the complexes and gradually increasing the concentration of CT-DNA ( $0.94\text{--}4.69 \times 10^{-5}$  M for **1** and **2**;  $1.88\text{--}6.57 \times 10^{-5}$  M for **3**;  $1.98\text{--}6.92 \times 10^{-5}$  M for **4**). The binding constant  $K_b$  was determined using the Eq. 1 (Vijayalakshmi et al. 2000):

$$[\text{DNA}] \times (\varepsilon_a - \varepsilon_f)^{-1} = [\text{DNA}] \times (\varepsilon_b - \varepsilon_f)^{-1} + K_b^{-1} \times (\varepsilon_b - \varepsilon_f)^{-1} \quad (1)$$

where  $\varepsilon_a$ ,  $\varepsilon_f$ ,  $\varepsilon_b$  are absorbance/[compound], extinction coefficient of the free compound and the extinction coefficient of the bound compound, respectively.

#### Fluorescence measurements

The competitive interactions of Ru(II) complexes **1**, **2**, **3** and **4** and the fluorescence probe either ethidium bromide (EB) or Hoechst 33258 (H), with CT-DNA, have been studied by measuring the change of fluorescence intensity of the probe–DNA solution after addition of the complex. Reaction mixtures containing 47  $\mu$ M of CT-DNA (calculated per phosphate) in 1 mL of 40 mM bicarbonate solution (pH 8.4) were pretreated with 1.5  $\mu$ L of 1% H probe solution (28  $\mu$ M final concentration) or 1  $\mu$ L of 1% EB solution (25  $\mu$ M final concentration) (in separate experiments) for 20 min and the mixture was analyzed by fluorescence measurement. The final DNA concentration was constant while the gradually increasing concentrations of the complexes (from 0.25 to  $11 \times 10^{-5}$  M in EB displacement and  $0.5\text{--}20 \times 10^{-6}$  M in H displacement) were successively added and the change in the fluorescence intensity was measured using a Thermo Scientific Lumina Fluorescence spectrometer (Finland) equipped with a 150 W Xenon lamp.

The slits on the excitation and emission beams were fixed at 10 nm. All measurements were performed by excitation at 350 nm for Hoechst 33258, and by excitation at 500 nm for EB in the range of 390–600 nm and 520–700 nm, respectively. The control was the probe–CT-DNA solution. Complexes of Ru(II) (**1**, **2**, **3** and **4**) did not have fluorescence under applied conditions. The obtained fluorescence quenching data were analyzed according to the Stern–Volmer equation (Lakowicz and Weber 1973): The obtained fluorescence quenching data were analyzed according to the Stern–Volmer Eq. (2)

$$I_0/I = 1 + K[Q] \quad (2)$$

where  $I_0$  and  $I$  represent the fluorescence intensities of probe–CT-DNA in the absence and presence of the complex, respectively,  $K$  is the quenching constant, and  $Q$  is the concentration of the corresponding complex. The  $K$  value is calculated from the ratio of the slope to the intercept from the plot of  $I_0/I$  versus  $[Q]$ .

Primary spectra of all spectrometric measurements were imported into OriginPro 2018.

For BSA fluorescence measurements, BSA concentration in 40 mM bicarbonate buffer was kept constant in all samples, while the concentration of the compounds was increased: in 1 mL of buffer 5  $\mu$ L of stock solution of BSA (3 mg/mL) and an aliquot of stock solution of the compound was added and incubated for 30 min and emission spectra in range 295 to 500 nm were recorded (excitation wavelength 280 nm). Aliquots of the solution of **1**, **2**, **3** and **4** were successively added at final concentrations of 2.5 to 20  $\mu$ M for **1** and **4**; 0.05 to 1.75  $\mu$ M for **2** and 2.5 to 25  $\mu$ M for **3**. The change in the fluorescence intensity was measured.

In order to avoid the effect of inner filter effect, very low concentrations of CT-DNA, BSA and the complexes are used (Tian et al. 2010).

#### DNA cleavage experiments

For DNA cleavage experiments the plasmid pUC19 (pUC19, 2686 bp, purchased from Sigma-Aldrich, USA) was prepared by its transformation in chemically competent cells *Escherichia coli* strain XL1 blue. Amplification of the clone was done according to the protocol for growing *E. coli* culture overnight in LB medium at 37 °C (Sambrook et al. 1989) and

purification was performed using Qiagen Plasmid plus Maxi kit. Finally, DNA was eluted in 10 mM Tris–HCl buffer and stored at – 20 °C. The concentration of plasmid DNA (1.16  $\mu$ g/ $\mu$ L) was determined by measuring the absorbance of the DNA-containing solution at 260 nm. One optical unit corresponds to 50  $\mu$ g/mL of double stranded DNA.

The cleavage reaction of supercoiled pUC19 DNA by Ru(II) complexes was investigated by incubation of different concentrations of the complexes with 550 ng of pUC19 in a 20  $\mu$ L reaction mixture in 40 mM bicarbonate buffer 8.4 at 37 °C, for 90 min. The reaction mixtures were vortexed from time to time. The reaction was terminated by a short centrifugation at 10,000 rpm and the addition of 7  $\mu$ L of loading buffer (0.25% bromophenol blue, 0.25% xylene cyanol FF and 30% glycerol in TAE buffer, pH 8.24 (40 mM Tris–acetate, 1 mM EDTA)). The samples were subjected to electrophoresis on 1% agarose gel (Amersham Pharmacia-Biotech, Inc) prepared in TAE buffer pH 8.24. The electrophoresis was performed at a constant voltage (80 V) until bromophenol blue had passed through 75% of the gel. A Submarine Mini-gel Electrophoresis Unit (Hoeffer HE 33) with an EPS 300 power supply was used. After electrophoresis, the gel was stained for 30 min by soaking it in an aqueous ethidium bromide solution (0.5  $\mu$ g/mL). The stained gel was illuminated under a UV transilluminator Vilber-Lourmat (France) at 312 nm and photographed with a Nikon Coolpix P340 Digital Camera through filter DEEP YELLOW 15 (TIFFEN, USA).

Primary spectra of all spectrometric measurements were imported into OriginPro 2018 and were processed by this software package.

#### Antimicrobial activity

The antibacterial activities of all compounds were evaluated against pathogenic strains by applying the broth dilution method (Pasdar et al. 2017; Nasiri Sovari and Zobi 2020). Five strains of Gram-positive bacteria (*Clostridium sporogenes*, *Micrococcus flavus*, *Bacillus subtilis*, *Sarcina lutea* and *Staphylococcus aureus*), and four strains of Gram-negative bacteria (*Salmonella enteritidis*, *Proteus vulgaris*, *Pseudomonas aeruginosa* and *E. coli*) were used in the experiments. A commercially available, semisynthetic, and broad-spectrum antibiotic Chloramphenicol was used as the positive control, while DMSO

served as a negative control. For determination of antibacterial activity each of the bacterial strains were cultured onto Mueller–Hinton broth (MHB) by incubation overnight at 37 °C. A sample of each culture was then diluted 40-fold in fresh MHB and added to each well of the compound-containing plates. Transparent sterile 96-well microtiter plates (NUNC) flat bottom clear wells were used for the experiments. 100 µL of fresh MHB were added in each well and 100 µL of each complex was added in the first column. Mixtures from the previous columns (100 µL) were withdrawn and added to the next column. 10 µL of bacterial inoculums were added to all wells then plates were covered and incubated at 37 °C for 24 h without shaking. Inhibition of bacterial growth was determined using media and DMSO as negative control and bacteria with Chloramphenicol as a positive control. The initial concentration of the complexes and chloramphenicol was 5 mg/L. MIC values were determined as the lowest concentration at which the growth was inhibited, with no visible growth by the eye.

#### Statistical analysis

All experimental results reported in the results and discussion sections were based on averaging results of repeated experimental runs (triplicates), with the SD ranging from 2 to 5% of the reported average. Statistical significance is confirmed by Student's t-test.

## Results and discussion

### DNA binding study

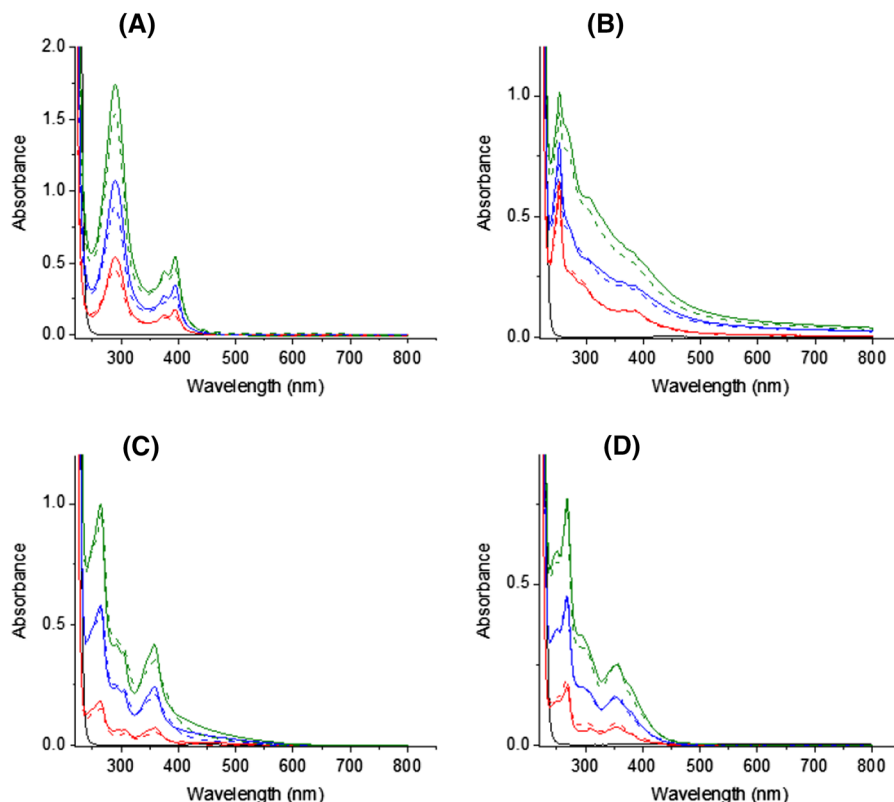
#### UV–Vis absorption study

Stability and solubility of arene ruthenium(II) complexes **1–4** were studied by UV–Vis spectroscopy. UV–Vis spectra of the complexes (at three different concentration) were recorded in the sodium bicarbonate buffer at different time intervals (0 and 2 h), which is a longer period of time than the reaction time of DNA binding study. The obtained results revealed no significant change in either the intensity or the position of absorption bands indicating their satisfactory stability under the experimental conditions (Fig. 1A–D).

DNA is one of the main targets of anticancer agents and it is well established that such compounds can bind to DNA both via covalent (Sherman et al. 1988) and/or non-covalent interactions. Non-covalent interactions include the interaction of a planar aromatic moiety between two base pairs of DNA via  $\pi$ -stacking, binding to the minor and major grooves of DNA, and electrostatic interactions with the negatively charged phosphate backbone (Strekowski and Wilson 2007). Hyperchromism and hypochromism are regarded as spectral evidence for DNA double-helix structural change when DNA reacts with other molecules (Keene et al. 2009). The hyperchromism originates from the disruption of the DNA duplex secondary structure and the hypochromism originates from the stabilization of the DNA duplex by either the intercalation binding mode or the electrostatic effect of small molecules (Li et al. 2012; Szekely and Gates 2006). The interaction of Ru(II) complexes with DNA was monitored spectrophotometrically. Figure 2A–D shows the UV–Vis absorbance spectra of CT-DNA (lines a) and **1**, **2**, **3**, and **4** before (lines b) and after interaction (lines d) with CT-DNA. Lines d in Fig. 2A–D represent calculated spectra and the percentage of hypochromism was determined from  $\{[(\epsilon_{\text{DNA}} + \epsilon_{\text{C}}) - \epsilon_{\text{b}}]/(\epsilon_{\text{DNA}} + \epsilon_{\text{C}})\} \times 100$ , where  $\epsilon_{\text{DNA}}$  is the extinction coefficient of CT-DNA,  $\epsilon_{\text{C}}$  is the extinction coefficient of free complex and  $\epsilon_{\text{b}}$  is the extinction coefficient of the bound complex (Vujčić Miroslava et al. 2013). The spectrum of CT-DNA displayed one absorption maximum at 259 nm and complex **1** displayed absorption maximum at a wavelength of 287 nm, and two smaller peaks at 374 nm and 393 nm (Fig. 2A, line b). Comparing the sum of absorbances at 259 nm of free complex **1** and free CT-DNA with the observed absorbance of the **1**–CT-DNA (Fig. 2A), the hypochromisms of 12%, 16% and 10% for all these bands, respectively, has been noticed. The obtained weak hypochromisms probably reflected changes in the conformation and structure of CT-DNA upon binding of the complex in the minor groove via planar part of the aromatic rings that favored electrostatic ( $\pi$ -anion) and hydrophobic ( $\pi$ -sigma) contacts with the exposed AT base pairs (Nikolić et al. 2019).

Complex **2** (Fig. 2B, line b) has a characteristic absorption band at 253 nm and three minor peaks at 348 nm, 366 nm and 384 nm. Upon the addition of **2**

**Fig. 1** UV–Vis spectra of **1** (A), complex **2** (B), complex **3** (C) and complex **4** (D) with varying concentrations of the complexes (1, 2 and 3  $\mu\text{M}$ , green, blue and red lines, respectively) at time interval of 0 h (solid lines) and 2 h (dashed lines). (Color figure online)



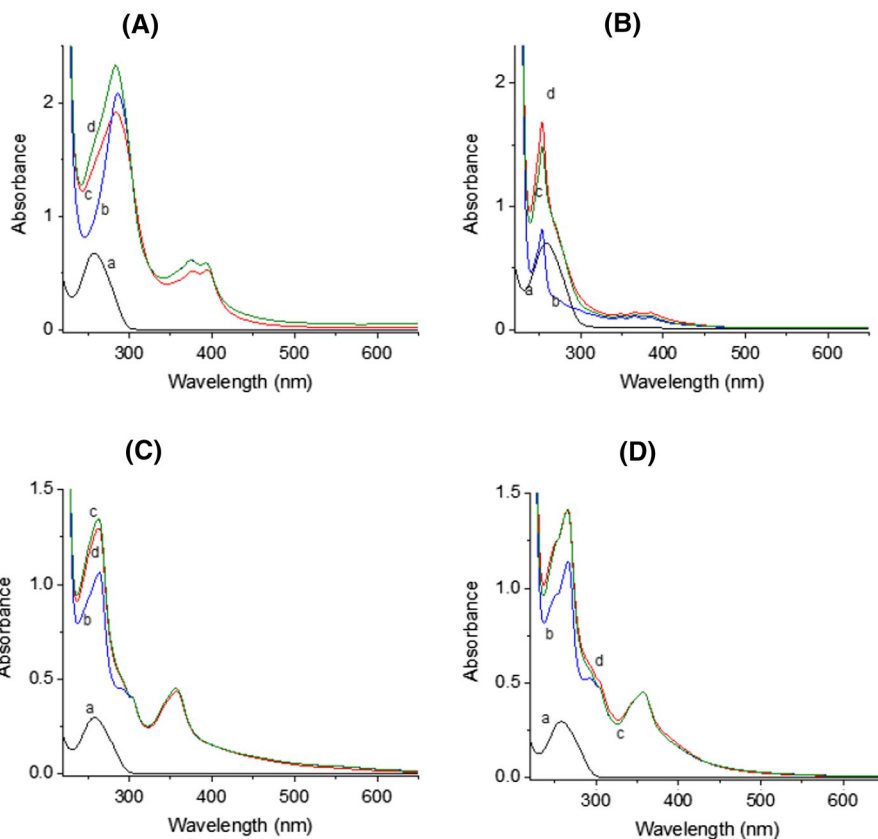
to CT-DNA, the band corresponding to **2**–CT-DNA (line d) was observed. No perturbations of the bands were observed in the visible region of the spectrum.

The absorption spectra of complexes **3** and **4** (lines b in Fig. 2C and D, respectively) exhibit intense absorption bands at about 263 nm and 357 nm as well as a shoulder at 285–302 nm. After interaction of CT-DNA with the complexes, no significant changes of the bands at 357 nm were assigned to ligand-to-metal charge transfer (LMCT), but the shoulder (assigned to the intra-ligand  $\pi$ – $\pi^*$  transition) flattened (lines d in Fig. 2C and D). The observed maximum at 265 nm and 267 nm in spectra of **3**–CT-DNA and **4**–CT-DNA, respectively, could be associated with overlapping of the absorption of nucleic base pairs and polypyridyl group from complexes **3** and **4**. Figure 2C and D suggest very close fit between the calculated and measured spectra of CT-DNA+complex mixtures indicating indicate only subtle changes in the structure of DNA after the interaction. These spectral changes accompanied by small hypochromism (4% and 0.5%, for **3**–CT-DNA and **4**–CT-DNA, respectively).

To obtain information on the stability of the newly formed complexes **1**–CT-DNA, **2**–CT-DNA, **3**–CT-DNA and **4**–CT-DNA, spectroscopic titration of the solution of all complexes with increasing concentration of CT-DNA was performed (Fig. 3A–D). The absorbances at 374 nm and 384 nm, for **1** and **2**, respectively, and at 357 nm for **3** and **4** were monitored for each concentration of DNA (insets in Fig. 3 show plots after linearization). The spectra shown in Fig. 3 are not subtracted by the absorbance of DNA and binding constants  $K_b$  of complex **1**, complex **2**, complex **3** and complex **4** were calculated using Eq. 1 (Vijayalakshmi et al. 2000). The values of  $4.97 \times 10^4 \text{ M}^{-1}$ ,  $2.75 \times 10^4 \text{ M}^{-1}$ ,  $1.043 \times 10^4 \text{ M}^{-1}$  and  $4.03 \times 10^4 \text{ M}^{-1}$ , respectively, were obtained. These values are lower for 2 orders of magnitude than those reported for classical intercalators i.e.,  $10^6$  to  $10^7 \text{ M}^{-1}$  (Cory et al. 1985) and comparable with results of previously published for Ru(II) based complexes (Ruiz et al. 2019; Colina-Vegas et al. 2015), suggesting non-intercalative binding interaction among complexes **1**, **2**, **3** and **4** and CT-DNA. The results indicate the interaction of all Ru(II) complexes with helix



**Fig. 2** Changes in UV–Vis absorption spectra of CT-DNA (9.89  $\mu\text{M}$ , curve a) after interaction with 3  $\mu\text{M}$  of complex **1** (A), complex **2** (B), complex **3** (C) and complex **4** (D). Curves b denote spectra of the complexes, curves c calculated spectra, and curves d spectra of complex–CT-DNA



DNA due to processes such as base modification and/or nick formation. An exception is complex **2** that can be partially intercalated between bases in the grooves due to properties of a planar aromatic anthryl-imidazol moiety which resulted in higher hypochromism, compared to the other complexes.

#### Fluorescence quenching study

To provide additional insight into the interactions between DNA and the Ru(II) complexes, the fluorescence spectrometry was performed by fluorescence competitive experiments with two different dyes: ethidium bromide (EB), a typical intercalator, and Hoechst 33258 (H), a minor groove binder. EB is known to be a planar cationic molecule that intercalates in a DNA double helix with a strong binding affinity (Garbett et al. 2004; Shi et al. 2011). The emission spectra of EB bound to CT-DNA in absence and presence **1**, **2**, **3** and **4** are given in Fig. 4A–D, respectively. The binding of EB to CT-DNA was followed by excitation at 500 nm with fluorescence maximum at 602 nm and

emits intense fluorescence due to its strong intercalation between the adjacent DNA base pairs. The addition of an increasing concentration of the Ru(II) complexes **1**, **2**, **3** and **4** to EB–CT-DNA system caused a significant reduction in fluorescence intensity of the band at 602 nm. The maximal decrease of EB–CT-DNA fluorescence intensity was 64% by **1** (Fig. 4A), 27% by **2** (Fig. 4B), 54% by **3** (Fig. 4C) and 37% by **4** (Fig. 4D), with the maximal applied concentration of the complex. In the work, Ru(II) complexes **1**, **2**, **3** and **4** had no obvious fluorescence under applied experimental conditions. The obtained results suggest that the complexes competed with EB in binding to DNA to a different extent. The extent of this quenching of EB by these complexes was estimated using the Stern–Volmer Eq. (2). The fluorescence quenching constant ( $K$ ) was calculated from the ratio of the slope to the intercept from the plot  $I_0/I$  versus [complex] as shown in the insets in Fig. 4. Some deviation of linearity of the plot  $I_0/I$  versus [1] ( $R^2=0.94$ ) (Fig. 4A) might be a consequence of stronger electrostatic interaction of the Ru(II)-arene complex cation (which

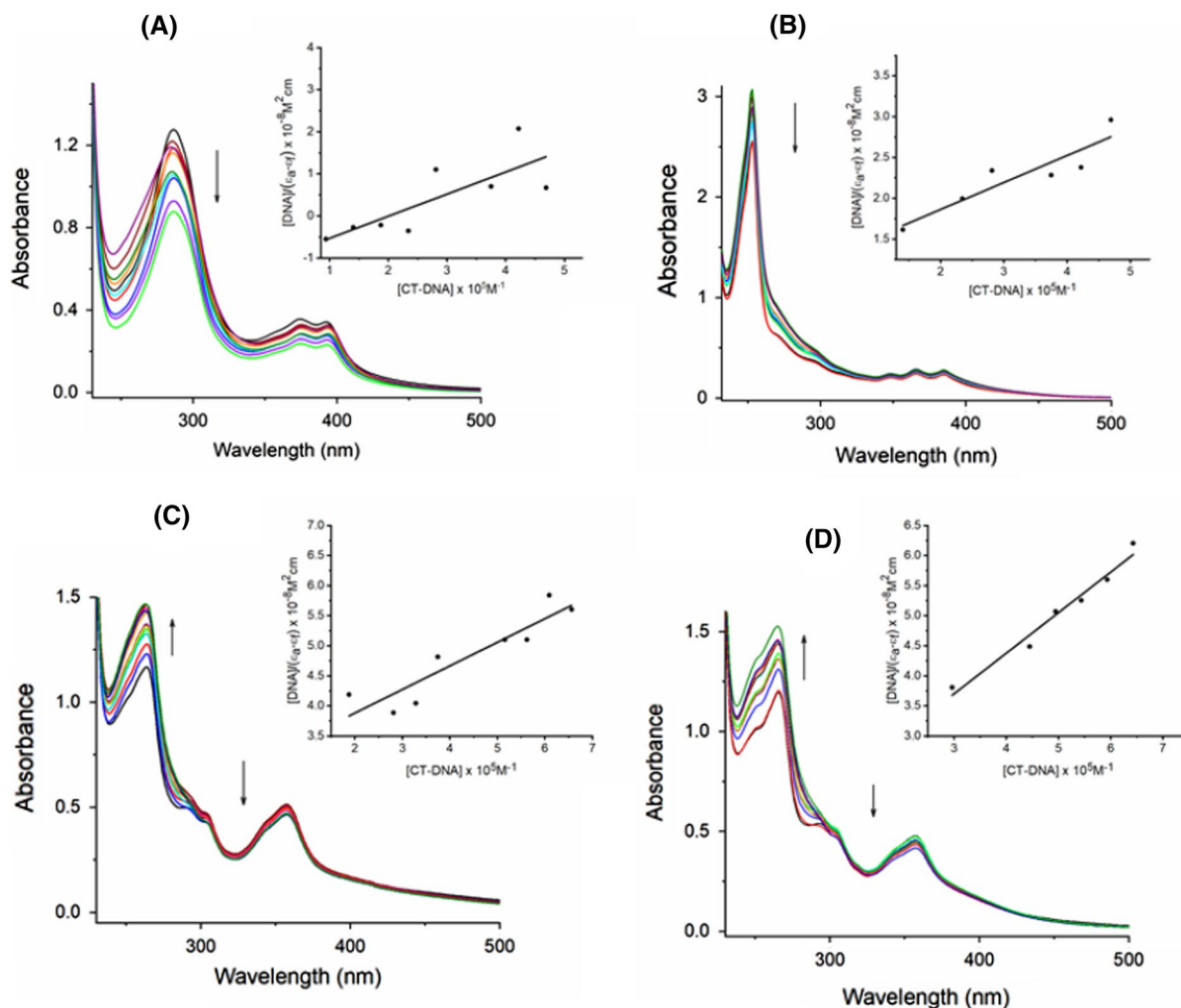


**Fig. 3** Absorption titration curves of complex **1** (A); complex **2** (B); complex **3** (C) and complex **4** (D) at fixed concentration (3  $\mu\text{M}$ ) with increasing concentrations of CT-DNA

in 40 mM bicarbonate buffer (pH 8.0). The arrows show the changes in absorbance upon increasing amounts of CT-DNA. Insets: plot of  $[\text{DNA}]/(\epsilon_{\text{A}} - \epsilon_{\text{F}})$  versus  $[\text{DNA}]$

formed in water environment) with DNA helix. By linear regression of the plots  $I_0/I$  versus  $[1]$ , the corresponding quenching constant  $K$  for Ru(II) complexes **1** was calculated as  $4.81 \times 10^4 \text{ M}^{-1}$ . The plots for **2** (Fig. 4B), **3** (Fig. 4C) and **4** (Fig. 4D) displayed a good linear relationship ( $R^2=0.99$ ) for the investigated concentration ranges, suggesting a singular mode of quenching and the corresponding quenching constant  $K$  were calculated as  $5.58 \times 10^3 \text{ M}^{-1}$ ,  $1.05 \times 10^4 \text{ M}^{-1}$  and  $4.85 \times 10^3 \text{ M}^{-1}$ , respectively. The results indicate the complex **1** had greater DNA binding propensity comparing to **2**, **3** and **4**. The structural changes in DNA arise from electrostatic binding by

the complexes, which reduce the binding affinity of EB (Spillane et al. 2007).

To further clarify the nature of interactions of the compounds with CT-DNA, a displacement study was performed with the minor groove binder Hoechst 33258. Hoechst 33258 (H) binds strongly and selectively with high affinity to double-stranded B-DNA structure and like other minor groove binders, it recognizes at least four AT base pairs. It binds by a combination of hydrogen bonding, van der Waals contacts with the walls of the minor groove and electrostatic interactions between its cationic structure and DNA (Kakkar et al. 2002). The binding of H 33,258 to



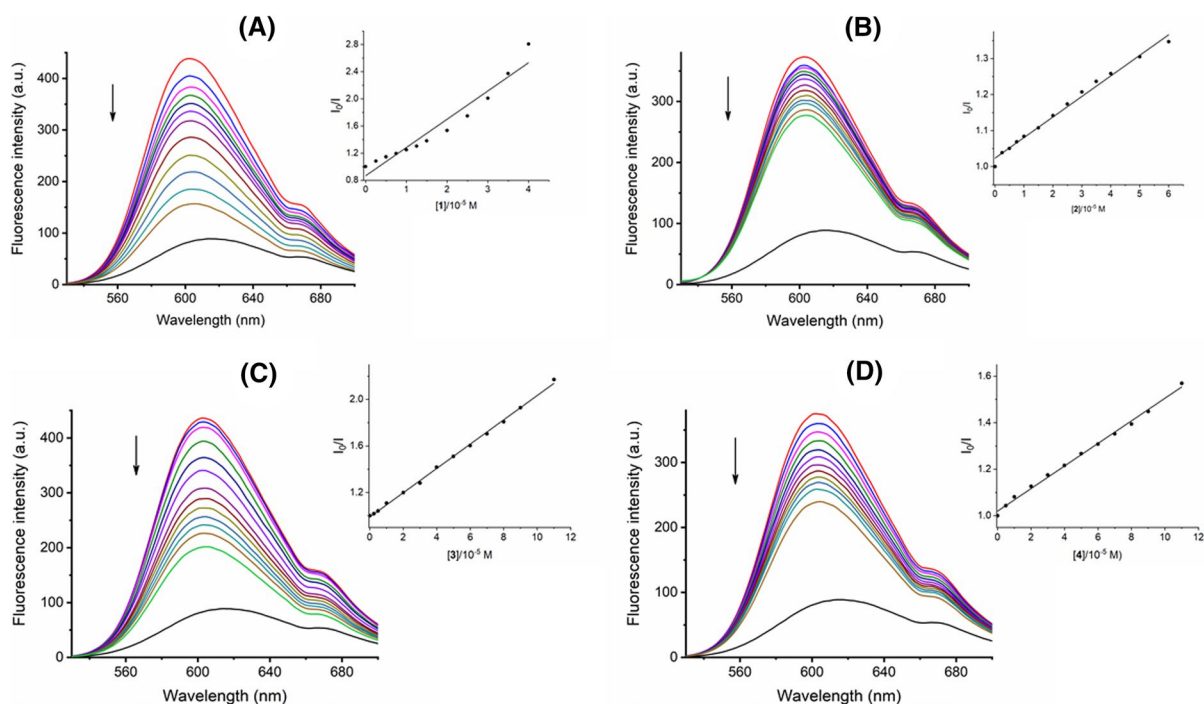


**Fig. 4** Fluorescence displacement study—changes in emission spectra of ethidium bromide (EB,  $2.5 \times 10^{-5}$  M) bound to CT-DNA ( $4.7 \times 10^{-5}$  M) and quenching EB—CT-DNA system by increasing concentrations of **1** (0.25, 0.5, 0.75, 1, 1.25, 1.5, 2, 2.5, 3, 3.5 and  $4 \times 10^{-5}$  M; panel A), **2** (0.25, 0.5, 0.75, 1, 1.25, 1.5, 2, 2.5, 3, 3.5, 4, 5 and  $6 \times 10^{-5}$  M; panel B), **3** (0.25, 0.5, 1, 2, 3, 4, 5, 6, 7, 8, 9 and  $11 \times 10^{-5}$  M; panel C) and **4** (0.25, 0.5, 1, 2, 3, 4, 5, 6, 7, 8, 9 and  $11 \times 10^{-5}$  M; panel D). The arrows show that fluorescence intensity decreased with

CT-DNA was followed by excitation at 350 nm with the maximum fluorescence at 443 nm. Figure 5A–D shows the characteristic changes in fluorescence emission spectra of H 33,258 after binding to the CT-DNA and changes in the fluorescence intensity after successively addition an increasing concentration of **1**, **2**, **3** and **4**. The obtained fluorescence quenching data were analyzed according to the Stern–Volmer Eq. (2) (Lakowicz and Weber 1973). The fluorescence intensity of the band at 443 nm of the H–CT-DNA system decreased by 75% with the maximal performed concentration of ligand **1** (Fig. 5A). The quenching constant was calculated by linear regression of a plot  $I_0/I$  against  $[Q]$  (Inset in Fig. 5A) as  $K_{sv} = 7.03 \times 10^5 \text{ M}^{-1}$  ( $R^2 = 0.98$ ). Fluorescence of the H–CT-DNA system upon binding complex **2** to CT-DNA was decreased by 66% and the corresponding quenching constant was calculated as  $1.03 \times 10^5 \text{ M}^{-1}$

increasing concentration of the complex. The insets show fluorescence quenching curves of ethidium bromide bound to DNA at  $\lambda_{\text{max}} = 602 \text{ nm}$  by **1** (Panel A), **2** (Panel B), **3** and **4** (Panel D). The quenching constants  $K_{sv}$  were calculated using Eq. (1) by linear regression of a plot  $I_0/I$  against  $[Q]$ , where  $I_0$  and  $I$  represent the fluorescence intensities of EB–CT-DNA in absence and presence of the complex, and  $[Q]$  is the concentration of the corresponding complex

( $R^2 = 0.99$ ). (Fig. 5B). When complex **3** was added to H–CT-DNA solution, a decrease of 55% was observed and the quenching constant was determined as  $K_{sv} = 2.24 \times 10^5 \text{ M}^{-1}$  ( $R^2 = 0.99$ ) (Fig. 5C). The fluorescence intensity of the band at 443 nm of the H–CT-DNA system decreased by 58% with the maximal performed concentration of **4** and corresponding constant  $K_{sv} = 2.03 \times 10^5 \text{ M}^{-1}$  ( $R^2 = 0.99$ ) calculated from the ratio of the slope to the intercept from the plot of  $I_0/I$  against  $[Q]$  (Fig. 5D). It can be concluded that fluorescence intensity of the band at 443 nm of the H–CT-DNA decreased remarkably (more than 50% of the initial value) at a maximal applied concentration of the complexes, indicating the propensity of  $[\text{Ru}(\eta^6\text{-arene})(\text{XY})\text{Cl}](\text{PF}_6)$  to bind to DNA minor groove. Insets in Fig. 5 show the plots demonstrating that quenching of H bound to CT-DNA by **1**, **2**, **3** and

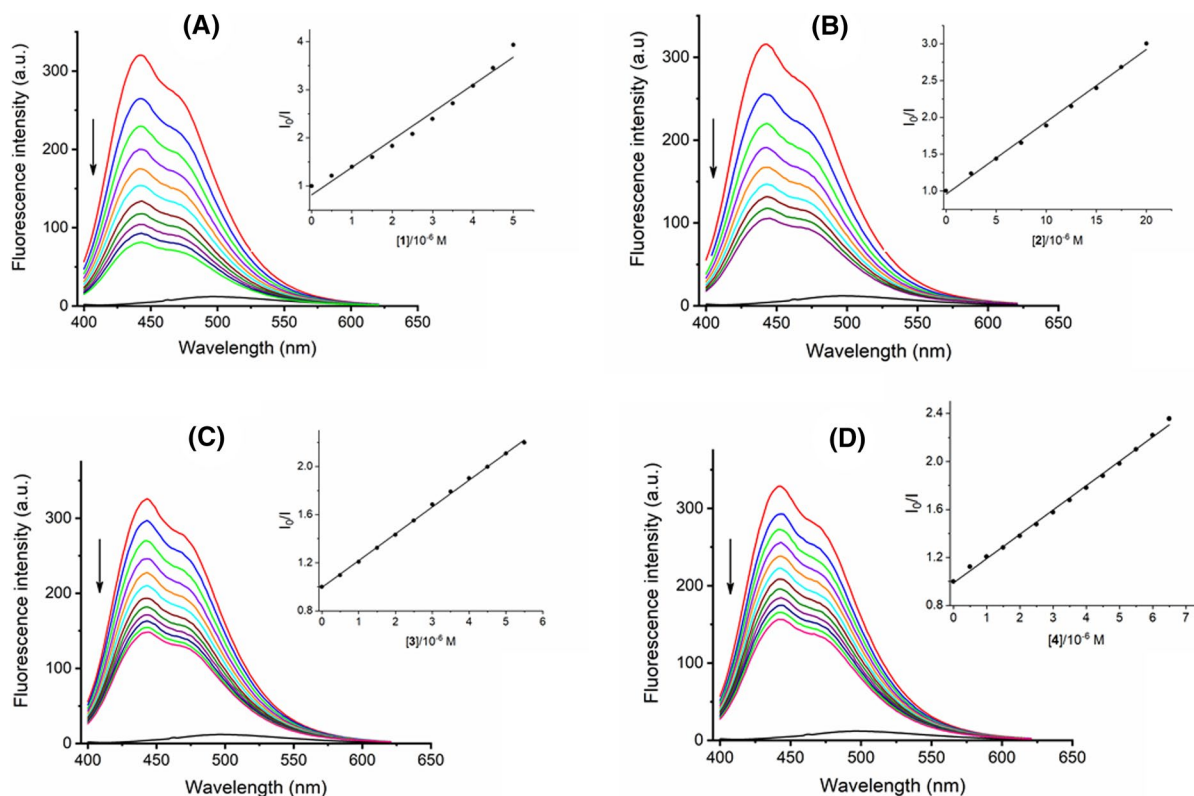


**Fig. 5** Fluorescence displacement study:— changes in emission spectra of Hoechst 33258 (H,  $2.5 \times 10^{-5}$  M) bound to CT-DNA ( $4.7 \times 10^{-5}$  M) and quenching H–CT-DNA system by increasing concentrations of **1** (0.5, 1, 1.5, 2, 2.5, 3, 3.5, 4, 4.5 and  $5 \times 10^{-6}$  M; panel **A**), **2** (2.5, 5, 7.5, 10, 12.5, 15, 17.5 and  $20 \times 10^{-6}$  M; panel **B**), **3** (0.5, 1, 1.5, 2, 2.5, 3, 3.5, 4, 4.5, 5 and  $5.5 \times 10^{-6}$  M; panel **C**) and **4** (0.5, 1, 1.5, 2, 2.5, 3, 3.5, 4, 4.5, 5, 5.5, 6 and  $6.5 \times 10^{-6}$  M; panel **D**). The arrows show that fluorescence intensity either decreased or increased with increas-

ing concentration of the complex. The insets show fluorescence quenching curves of H bound to DNA at  $\lambda_{\max} = 443$  nm by **1** (Panel **A**), **2** (Panel **B**), **3** and **4** (Panel **D**). The quenching constants  $K_{sv}$  were calculated using Eq. (1) by linear regression of a plot  $I_0/I$  against  $[Q]$ , where  $I_0$  and  $I$  represent the fluorescence intensities of H–CT-DNA in absence and presence of the complex, and  $[Q]$  is the concentration of the corresponding complex

**4** agrees with the linear Stern–Volmer Eq. (2) for the investigated concentration ranges of the complexes.

Comparing the  $K$  values, it may be concluded that complex **1** carrying *p*-cymene as an arene was more efficient as a DNA binder than the other two complexes (**2** and **4**) and from complex **3** (with toluene as arene moiety), suggesting that structural differences in aromatic moiety contributed to binding with the macromolecule.

#### Plasmid DNA interaction study

The type of DNA metal complex interactions has been further established by investigation of damage to circular plasmid DNA using an agarose gel

electrophoretic assay. The assay allows assessment of DNA strand cleavage by monitoring the conversion of compact circular supercoiled form DNA (FI) into a more relaxed, open form FII and linear form FIII. These three conformations are distinguishable when subjected to agarose gel electrophoresis. Relative fast migration is observed for supercoiled form FI, while open circular form FII migrates slowly, and linear form FIII migrates between FI and FII. The abilities of ruthenium(II)-arene complexes **1**, **2**, **3** and **4** to cleave plasmid pUC19 DNA were investigated. As shown in Fig. 6A–D (lanes 1) plasmid pUC19 consisted mainly of supercoiled form FI and nicked form FII, with an also small quantity of linear form FIII. Upon addition of complex **1** to the plasmid, changes

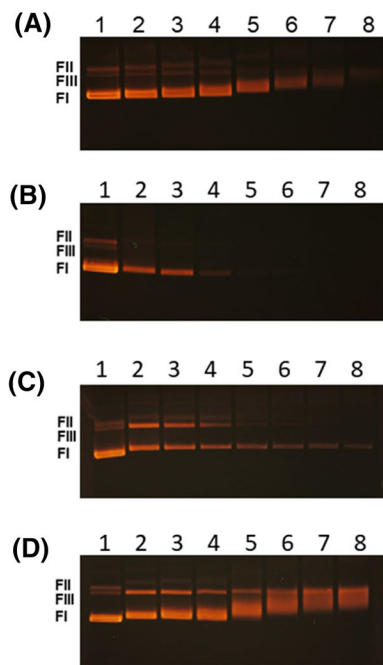


**Fig. 6** DNA cleavage activity of Ru(II)-arene complexes: the agarose gel electrophoretic pattern of supercoiled form FI, open form FII and linear form FIII of pUC19 (0.34  $\mu$ M; lanes 1) after an interaction with **1** (gel **A**—0.0125, 0.025, 0.05, 0.1, 0.15, 0.2 and 0.25 mM concentration, lanes 2–8, respectively); **2** (gel **B**—0.0625, 0.0125, 0.25, 0.375, 0.5, 0.625 and 0.75 mM concentration, lanes 2–8, respectively); **3** (gel **C**—0.25, 0.5, 1, 1.5, 2, 2.5 and 3 mM concentration, lanes 2–8, respectively) and **4** (gel **D**—0.0625, 0.125, 0.25, 0.5, 0.75, 0.875 and 1 mM concentration, lanes 2–8, respectively)

in the intensity of fluorescence of ethidium bromide and mobility of a supercoiled form of pUC19 were observed in comparison to the control (Fig. 6A, lane 1). The absence of linear forms indicates that Ru(II) complex **1** has no nuclease activity. The interaction of complex **1** with plasmid produces conformational changes of supercoiled circular DNA in concentration dependent way. Additionally, the increase in the concentration of complex **1** already from 0.025 mM (Fig. 6A, lane 3) produced the appearance of indistinguishable small fragments of DNA resulting in the smear in the gel (Fig. 6A, lanes 4–7). At maximal performed concentration (0.25 mM, Fig. 6A, lane 8) the fluorescence of the electrophoretic band almost completely disappears. No strand scission was observed at increasing concentration of complex **2** (Fig. 6B, lane 2–8). At a concentration of 0.25 mM, the fluorescence of the electrophoretic band (Fig. 6B,

lane 4) almost completely disappeared. Upon addition of complex **3** (Fig. 6C, lanes 2–8) to the plasmid pUC19, the conversion of supercoiled DNA in a concentration dependent double strand scission into linear forms FIII was observed. The result indicates strong nuclease activity of complex **3**.

As can be seen in Fig. 6D, a decrease in the mobility of the FI form on the gel in comparison to the control (lane 1) and the appearance of band smears on concentration-dependent way is due to nuclease activity of complex **4**. The conversion of FI form into form FIII was much more efficient with much less applied concentration (0.0625–1 mM, Fig. 6D, lanes 2–8, respectively), compared to other complexes.

From the obtained results it can be concluded that all complexes exhibit strong concentration-dependent cleavage activity of supercoiled DNA molecules. Considering the concentration of the complexes required to completely conversion of plasmid pUC19 and the electrophoretic pattern, it can be concluded that the most pronounced effect on supercoiled circular DNA has complex **1**, followed by complex **2**, then complex **4** and the least activity showed complex **3**.

#### Interaction with BSA

BSA has often been used as a model protein to measure the albumin-binding ability of drugs and metal complexes. Figure 7 shows that BSA exhibited an intense fluorescence emission band at 332 nm when excited at 280 nm, due to the presence of tryptophan residues Trp-134 and Trp-212 (Protogeraki et al. 2014). The addition of increasing concentrations of complexes **1**, **2**, **3** or **4** to BSA solution resulted in a significant quenching of fluorescence intensity by 71%, 53%, 72% and 64%, respectively indicating the interaction of the complexes with protein (Fig. 5A–D). The obtained strong decrease in fluorescence intensity at maximum wavelength suggested that the complex caused conformational changes in the secondary structure of albumin which led to a more hydrophobic, less exposed to the solvent, the tryptophan residue present in the hydrophobic cavity of the protein. The effect of complex **3** and **1** were the greatest, followed by complex **4** and finally **2**. The fluorescence quenching data were further analyzed with the Stern–Volmer Eq. (3) as follows (Lakowicz and Weber 1973).

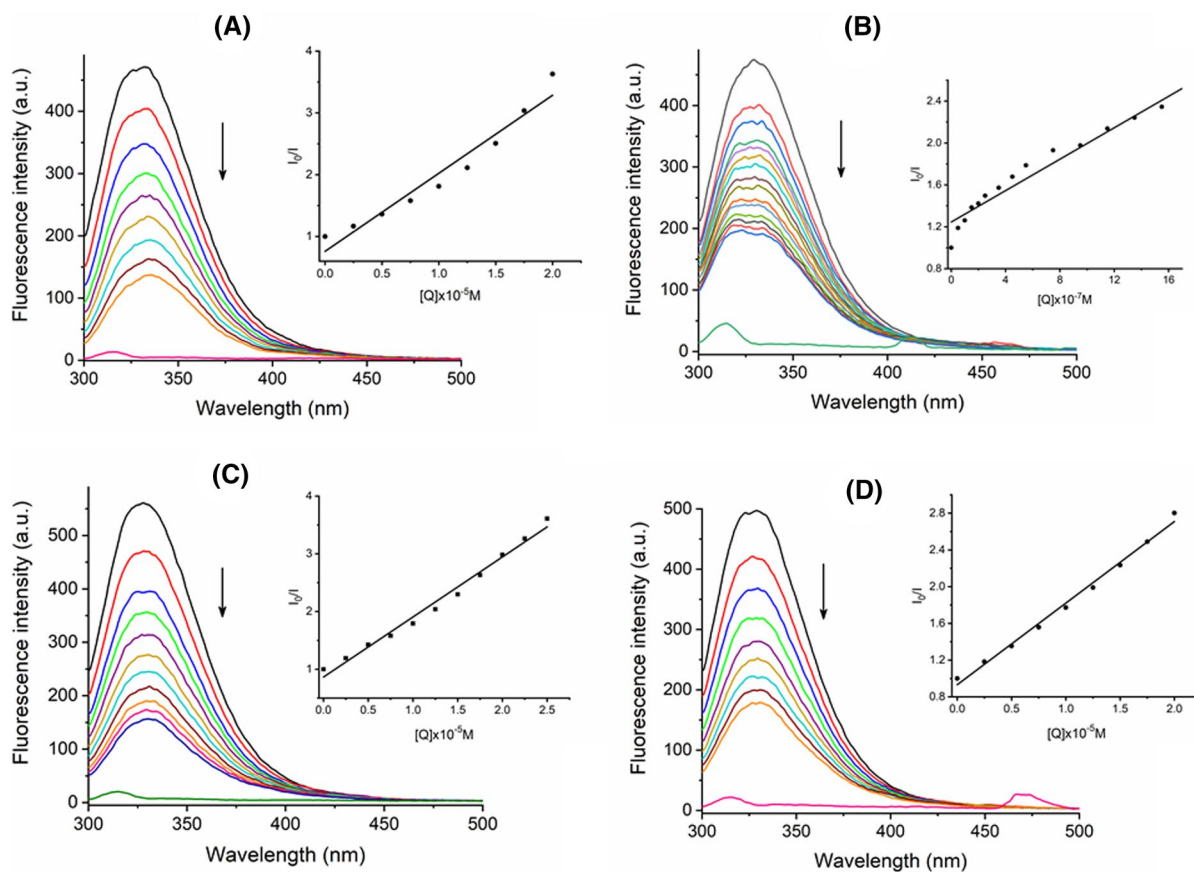


**Fig. 7** Fluorescence spectra of BSA in the absence and presence of increasing concentrations of **1**, **2**, **3** and **4** (panels **A**, **B**, **C** and **D**, respectively). Values of  $K_{sv}$  were calculated from

$$I_0/I = 1 + k_q \tau_0 [Q] = 1 + K_{sv} [Q] \quad (3)$$

$$K_q = K_{sv} / \tau_0 \quad (4)$$

where  $I$  and  $I_0$  are the steady state fluorescence intensities in the presence and absence of a quencher, respectively.  $K_{sv}$  is the Stern–Volmer constant and  $[Q]$  is a concentration of the quencher *i.e.*, the complex;  $\tau_0$  is the average lifetime of the protein without the quencher. As shown in insets in Fig. 5, good linear fitting linearity ( $R^2 > 0.95$ ) of the plot suggests that the Stern–Volmer model is appropriate for studying the binding mechanism between the Ru(II) complexes and BSA. Stern–Volmer constant  $K_{sv}$  was calculated from the plot  $I_0/I$  versus  $[\text{complex}]$  using Eq. (3). The results interaction of **1** (Fig. 7A), **2** (Fig. 7B), **3**

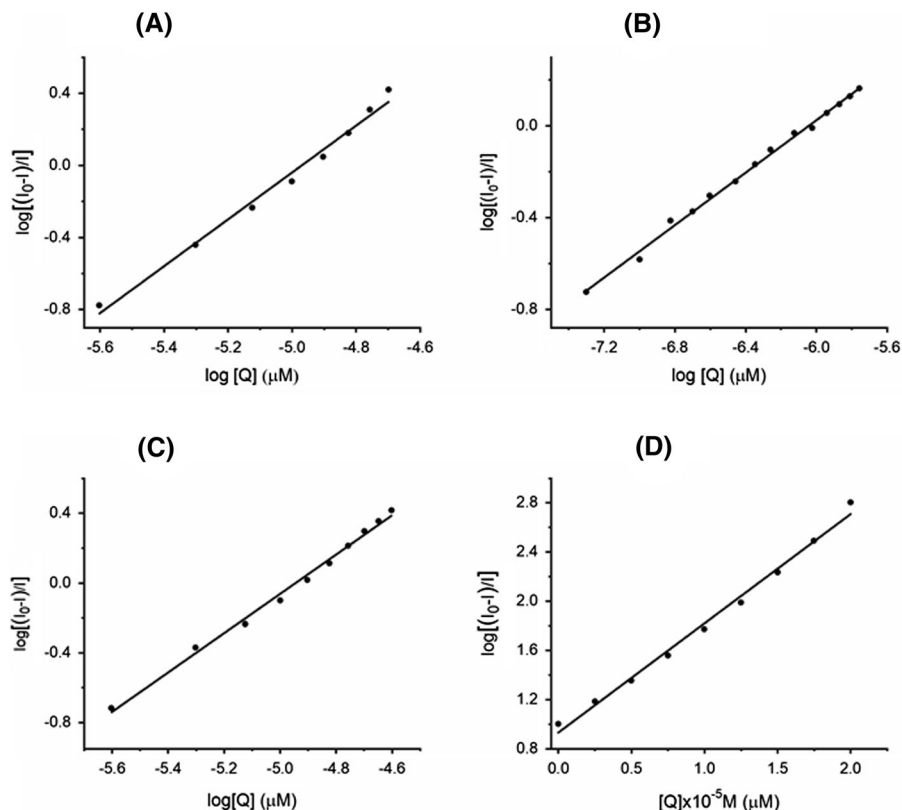
the plot  $I_0/I$  versus  $[Q]$  shown in insets. The arrows show the decreasing in fluorescence intensities with increasing concentrations of the compounds

(Fig. 7C) and **4** (Fig. 7D) with BSA are summarized in Table 1. A linear Stern–Volmer plot is generally indicative of a single class of fluorophores, all equally accessible to the quencher, and as can be seen in an inset on Fig. 7D, BSA can be quenched both by collision and by complex formation with **4**. In case of **1** (inset on Fig. 7A) and **3** (inset on Fig. 7C), the

**Table 1** The fluorescence quenching data for binding **1**, **2**, **3** and **4** to BSA

Complex	$K_{sv} (M^{-1})$	$K_q (M^{-1} s^{-1})$
<b>1</b>	$1.66 \times 10^5$	$1.66 \times 10^{13}$
<b>2</b>	$6.02 \times 10^5$	$6.02 \times 10^{13}$
<b>3</b>	$1.20 \times 10^5$	$1.20 \times 10^{13}$
<b>4</b>	$0.95 \times 10^5$	$0.95 \times 10^{13}$

**Fig. 8** Determination of  $K_b$  values for **1** (A), **2** (B), **3** (C) and **4** (D) from the plots of  $\log [(I_0 - I)/I]$  versus  $\log$  [complex]



Stern–Volmer plot exhibit an upward curvature and in the case of **2** (inset on Fig. 7B) the plot exhibits a downward curvature at high  $[Q]$ , followed modified form of the Stern–Volmer equation (Papadopoulou et al. 2005)

$$I_0/I = (1 + K_D[Q])(1 + K_S[Q]) \quad (5)$$

where  $K_D$  and  $K_S$  are, the dynamic and static quenching constants respectively. These observations suggest that quenching can occur by dynamic and static fluorescence quenching mechanisms. Static quenching can be caused also by the formation of a complex between the Ru(II) complexes and BSA that does not fluorescence by returning to an excited state. Using Eq. (4), the values of bimolecular quenching constant  $K_q$  for **1**, **2**, **3** and **4** calculated from  $K_{SV}$  and  $\tau_0$  assuming that the average lifetime of the biomolecule is around  $10^{-8} \text{ s}^{-1}$  (Banerjee et al. 2009) and presented in Table 1. The values are greater than the maximum value for dynamic quenching ( $2.0 \times 10^{10} \text{ M}^{-1} \text{ s}^{-1}$ ) (Shi et al. 2011), indicating static quenching mechanism by present Ru(II) complexes i.e., formation of

nonfluorescent complex forms between the complex and BSA.

During the static quenching process, the relation between the fluorescence intensity and concentration of quenching can be described as in Eq. (6) (Ghosh et al. 2016)

$$\log [(I_0 - I)/I] = \log K_b + n \log [Q] \quad (6)$$

where  $K_b$  denotes a degree of interaction of the protein with quencher and  $n$  is the number of binding sites. The values of  $K_b$  have been derived from the plots of  $\log [(I_0 - I)/I]$  versus  $\log$  [complex] for **1**, **2**, **3** and **4** (Fig. 8A–D) were calculated as  $2.01 \times 10^5 \text{ M}^{-1}$ ,  $1.65 \times 10^5 \text{ M}^{-1}$ ,  $2.02 \times 10^5 \text{ M}^{-1}$  and  $2.04 \times 10^5 \text{ M}^{-1}$ , respectively.

The obtained results showed a similar strong binding propensity of the tested Ru(II) complexes with BSA and confirmed the previous conclusion that a hydrophobic interaction takes place between BSA and the compound.



**Table 2** Minimal inhibitory concentration values ( $\mu\text{g}/\text{mL}$ ) for Ru complexes against pathogenic strains

Compound	Gram-positive					Gram-negative			
	<i>C. sporogenes</i>	<i>M. flavus</i>	<i>B. subtilis</i>	<i>S. lutea</i>	<i>S. aureus</i>	<i>S. enteritidis</i>	<i>P. aeruginosa</i>	<i>P. vulgaris</i>	<i>E. coli</i>
Complex <b>1</b>	39	39	19.5	78	19.5	39	78	39	1.22
Complex <b>2</b> *	–	–	–	–	–	–	–	–	–
Complex <b>3</b>	78	312.5	–	625	312.5	312.5	312.5	78	312.5
Complex <b>4</b>	625	> 1000	> 1000	> 1000	625	> 1000	> 1000	625	625
Chloramphenicol	19.5	19.5	4.88	19.5	19.5	19.5	39	19.5	9.76
DMSO	> 1000	> 2000	> 1000	> 1000	> 1000	> 1000	> 1000	> 2000	> 1000

\*There are no measurable results for complex 2 because of very low solubility of the compound in MHB media

### Antimicrobial activity

The high cytotoxic activity of Ru(II) complexes against cervical (HeLa) and breast (MDA-MB-231) cancer cells was proved (Nikolić et al. 2016), and its further biological activity need to be investigate. The antimicrobial activity of ruthenium complexes **1–4** was determined against selected reference strains of bacteria—*C. sporogenes*, *M. flavus*, *B. subtilis*, *S. lutea* and *S. aureus* (Gram-positive); *S. enteritidis*, *P. vulgaris*, *P. aeruginosa* and *E. coli* (Gram-negative) by broth microdilution method. The antibacterial activities of all the complexes were compared to the standard drug—chloramphenicol. The results are summarized in Table 2.

Complex **1** showed the best antimicrobial activity compared to other tested complexes and was comparable to Chloramphenicol against all selected pathogenic strains. In addition, this complex showed better antimicrobial activity against *E. coli* than Chloramphenicol. Complex **3** also demonstrated good antimicrobial activity against all tested pathogenic strains, opposite to complex **4** which had weak antimicrobial activity. The tested ruthenium complexes showed very similar MIC values against all nine tested pathogenic strains and this result rarely could be found in the literature. The most of ruthenium complexes represented in literature shown good activity against some bacterial strains, but weak or no activity against other strains (Kumar et al. 2016; Liao et al. 2017; Li et al. 2016). However, the complexes investigated in this paper showed similar activity against nine different pathogenic bacterial strains.

### Conclusion

The main purpose of this work was to investigate the effect of biologically active previously synthesized arene ruthenium(II) complexes ( $([\eta^6\text{-}p\text{-cymene})\text{Ru}(\text{Me}_2\text{dppz})\text{Cl}]\text{PF}_6$  (**1**) with  $\text{Me}_2\text{dppz} = 11,12\text{-dimethyldipyrido}[3,2\text{-}a:2',3'\text{-}c]$  phenazine,  $([\eta^6\text{-}p\text{-cymene})\text{Ru}(\text{aip})\text{Cl}]\text{PF}_6$  (**2**) with  $\text{aip} = 2\text{-}(9\text{-anthryl})\text{-}1H\text{-imidazo}[4,5\text{-}f][1,10]$  phenanthroline),  $([\eta^6\text{-toluene})\text{Ru}(\text{ppf})\text{Cl}]\text{PF}_6$  (**3**) and  $([\eta^6\text{-}p\text{-cymene})\text{Ru}(\text{ppf})\text{Cl}]\text{PF}_6$  (**4**) with  $\text{ppf} = \text{pyrido}[2',3':5,6]$  pyrazino[2,3-*f*][1,10]phenanthroline on DNA and BSA. Spectrophotometric studies showed that all complexes interact with CT-DNA with moderate activity. Complexes **1**, **3** and **4** possible interact with A-T reach region of minor groove due to phenazine phenanthroline moieties in way that planar part of the aromatic rings made favorable electrostatic ( $\pi$ -anion) and hydrophobic ( $\pi$ -sigma) interactions with DNA functional groups. Complex **2** can be partially intercalated between bases in the groove due to a planar anthryl aromatic-imidazol moiety. The fluorescence competition study with the intercalator ethidium bromide and the minor groove binder Hoechst 33258, also demonstrated that differences in aromatic moiety contribute to binding in the: **1** carrying *p*-cymene as an arene was more efficient as a groove binder than the other two complexes (**2** and **4**) and than complex **3** (with toluene as arene moiety). The gel electrophoresis results showed that the complexes have nuclease activity and produced conformational changes of supercoiled circular plasmid



DNA on strong concentration-dependent way. The most pronounced effect on supercoiled circular DNA has complex **1** bearing *p*-cymene. Without any doubt Ru(II) ion is very important for damaging activity of the complexes, however, complex anions can also affect results substantially and more studies are needed to better understand this process. Interactions of studied complexes on the protein model system (BSA) showed that all Ru(II) complexes under study strongly bind to BSA and the intrinsic fluorescence of BSA was quenched through static quenching mechanism. All the complexes showed a significant antibacterial activity. Considering previously reported cytotoxic activity (Nikolić et al. 2016; Pavlović et al. 2019) it can be concluded that DNA damage is at least in part, responsible for the activity of the complexes. Additionally, interaction with BSA suggested that the complexes are suitable for distribution and transportation as potential DNA targeting drugs.

**Acknowledgements** The authors are grateful to the Ministry of Education, Science and Technological Development of the Republic of Serbia for the financial support (Grant Nos. 451-03-68/2022-14/200026; 451-03-68/2022-14/200168; 451-03-68/2022-14/200288).

#### Declarations

**Conflict of interest** No potential conflict of interest was reported by the authors.

#### References

- Alessio E, Messori L (2019) NAMI-A and KP1019/1339, two iconic ruthenium anticancer drug candidates face-to-face: a case story in medicinal inorganic chemistry. *Molecules* 24:1995–2015. <https://doi.org/10.3390/molecules24101995>
- Ascone I, Messori L, Casini A, Gabbiani C, Balerna A, Dell'Unto F, Castellano AC (2008) Exploiting soft and hard X-ray absorption spectroscopy to characterize metal-drug/protein interactions: The binding of [trans-RuCl<sub>4</sub>(Im)(dimethylsulfoxide)] [ImH] (Im = imidazole) to bovine serum albumin. *Inorg Chem* 47:8629–8634. <https://doi.org/10.1021/ic8001477>
- Banerjee P, Pramanik S, Sarkar A, Bhattacharya SC (2009) Deciphering the fluorescence resonance energy transfer signature of 3-pyrazolyl 2-pyrazoline in transport proteinous environment. *J Phys Chem B* 113:11429–11436. <https://doi.org/10.1021/jp811479r>
- Colina-Vegas L, Villarreal W, Navarro M, de Oliveira CR, Graminha AE, da Maia PI, Deflon VM, Ferreira AG, Cominetti MR, Batista AA (2015) Cytotoxicity of Ru(II) piano-stool complexes with chloroquine and chelating ligands against breast and lung tumor cells: Interactions with DNA and BSA. *J Inorg Biochem* 153:150–161. <https://doi.org/10.1016/j.jinorgbio.2015.07.016>
- Cory M, McKee DD, Kagan J, Henry DW, Miller JA (1985) Design, synthesis, and DNA binding properties of bifunctional intercalators. Comparison of polymethylene and diphenyl ether chains connecting phenanthridine. *J Chem Am Soc* 107:2528–2536. <https://doi.org/10.1021/ja00294a054>
- Fangfei L, Collins JG, Keene FR (2015) Ruthenium complexes as antimicrobial agents. *Chem Soc Rev* 44:2529–2542. <https://doi.org/10.1039/c4cs00343h>
- Garbett NC, Hammond NB, Graves DE (2004) Influence of the amino substituents in the interaction of ethidium bromide with DNA. *Biophys J* 87:3974–3981. <https://doi.org/10.1529/biophysj.104.047415>
- Ghosh K, Rathi S, Arora D (2016) Fluorescence spectral studies on interaction of fluorescent probes with Bovine Serum Albumin (BSA). *J Lumin* 175:135–140. <https://doi.org/10.1016/j.jlumin.2016.01.029>
- Go RS, Adjei AA (1999) Review of the comparative pharmacology and clinical activity of cisplatin and carboplatin. *J Clin Oncol* 17:409–422. <https://doi.org/10.1200/JCO.1999.17.1.409>
- <https://www.accessdata.fda.gov/scripts/cder/daf/index.cfm?event=reportsSearch.process&rptName=2&reportSelectMonth=12&reportSelectYear=1978&nav>
- Kakkar R, Garg R, Suruchi (2002) Towards understanding the molecular recognition process in Hoechst–DNA complexes. *J Mol Struct* 584:37–44. [https://doi.org/10.1016/S0166-1280\(02\)00026-X](https://doi.org/10.1016/S0166-1280(02)00026-X)
- Keene FR, Smith JA, Collins JG (2009) Metal complexes as structure-selective binding agents for nucleic acids. *Coord Chem Rev* 253:2021–2035. <https://doi.org/10.1016/j.ccr.2009.01.004>
- Kelland L (2007) The resurgence of platinum-based cancer chemotherapy. *Nat Rev Cancer* 7:573–584. <https://doi.org/10.1038/nrc2167>
- Kumar SV, Scottwell SØ, Waugh E, McAdam CJ, Hanton LR, Brooks HJL, Crowley JD (2016) Antimicrobial properties of tris(homoleptic) ruthenium(II) 2-pyridyl-1,2,3-triazole “Click” complexes against pathogenic bacteria, including methicillin-resistant *Staphylococcus aureus* (MRSA). *Inorg Chem* 55:9767–9777. <https://doi.org/10.1021/acs.inorgchem.6b01574>
- Lakowicz JR, Weber G (1973) Quenching of fluorescence by oxygen. A probe for structural fluctuations in macromolecules. *Biochemistry* 12:4161–4170. <https://doi.org/10.1021/bi00745a020>
- Lee TY, Suh J (2009) Artificial proteases toward catalytic drugs for amyloid diseases. *Pure Appl Chem* 81:255–262. <https://doi.org/10.1351/PAC-CON-08-07-02>
- Lee SY, Kim CY, Nam T-G (2020) Ruthenium complexes as anticancer agents: a brief history and perspectives. *Drug Des Dev Ther* 14:5375–5392. <https://doi.org/10.2147/DDDT.S275007>
- Li X-L, Hu Y-J, Wang H, Yu B-Q, Yue H-L (2012) Molecular spectroscopy evidence of berberine binding to DNA: comparative binding and thermodynamic profile of intercalation. *Biomacromol* 13:873–880. <https://doi.org/10.1021/bm2017959>

- Li X, Heimann K, Li F, Warner JM, Keene RF, Collins JG (2016) Dinuclear ruthenium(II) complexes containing one inert metal centre and one coordinatively-labile metal centre: syntheses and biological activities. *Dalton Trans* 45:4017–4029. <https://doi.org/10.1039/C5DT04885K>
- Liao G, Ye Z, Liu Y, Fu B, Fu C (2017) Octahedral ruthenium(II) polypyridyl complexes as antimicrobial agents against mycobacterium. *PeerJ* 5:e3252. <https://doi.org/10.7717/peerj.3252>
- Lin K, Zhao Z-Z, Bo H-B, Hao X-J, Wang J-Q (2018) Applications of ruthenium complex in tumor diagnosis and therapy. *Front Pharmacol* 9:1323–1333. <https://doi.org/10.3389/fphar.2018.01323>
- Mantri Y, Lippard SJ, Baik M-H (2007) Bifunctional binding of cisplatin to DNA: why does cisplatin form 1,2-intra-strand cross-links with AG but not with GA? *J Am Chem Soc* 129:5023–5030. <https://doi.org/10.1021/ja067631z>
- Mari C, Pierroz V, Ferrari S, Gasser G (2015) Combination of Ru(II) complexes and light: new frontiers in cancer therapy. *Chem Sci* 6:2660–2686. <https://doi.org/10.1039/c4sc03759f>
- Nasiri Sovari S, Zobi F (2020) Recent studies on the antimicrobial activity of transition metal complexes of groups 6–12. *Chemistry (easton)* 2:418–452. <https://doi.org/10.3390/chemistry2020026>
- Nikolić S, Rangasamy L, Gligorijević N, Arandelović S, Radulović S, Gasser G, Grgurić-Šipka S (2016) Synthesis, characterization and biological evaluation of novel Ru(II)-arene complexes containing intercalating ligands. *J Inorg Biochem* 160:156–165. <https://doi.org/10.1016/j.jinorgbio.2016.01.005>
- Nikolić S, Grgurić-Šipka S, Djordjević IS, Dahmani R, Dekanski D, Vidičević S, Tošić J, Mitić D, Grubišić S (2019) Half-sandwich ruthenium(II)-arene complexes: synthesis, spectroscopic studies, biological properties, and molecular modeling. *J Coord Chem* 72:148–163. <https://doi.org/10.1080/00958972.2018.1553298>
- Notaro A, Gasser G (2017) Monomeric and dimeric coordinatively saturated and substitutionally inert Ru(II) polypyridyl complexes as anticancer drug candidates. *Chem Soc Rev* 46:7317–7337. <https://doi.org/10.1039/c7cs00356k>
- Papadopoulou A, Green RJ, Frazier RA (2005) Interaction of flavonoids with bovine serum albumin: a fluorescence quenching study. *J Agric Food Chem* 53:158–163. <https://doi.org/10.1021/jf048693g>
- Pasdar H, Saghavaz BH, Foroughifar N, Davallo M (2017) Synthesis, characterization and antibacterial activity of novel 1,3-diethyl-1,3-bis(4-nitrophenyl)urea and its metal(II) complexes. *Molecules* 22:2125. <https://doi.org/10.3390/molecules22122125>
- Pavlović M, Nikolić S, Gligorijević N, Dojčinović B, Arandelović S, Grgurić-Šipka S, Radulović S (2019) New organoruthenium compounds with pyrido[2',3':5,6]pyrazino[2,3-f][1,10]phenanthroline: synthesis, characterization, cytotoxicity and investigation of mechanism of action. *J Biol Inorg Chem* 24:297–310. <https://doi.org/10.1007/s00775-019-01647-4>
- Protogeraki C, Andreadou EG, Perdih F, Turel I, Pantazaki AA, Psomas G (2014) Cobalt(II) complexes with the antimicrobial drug enrofloxacin: Structure, antimicrobial activity, DNA- and albumin-binding. *Eur J Med Chem* 86:189–201. <https://doi.org/10.1016/j.ejmech.2014.08.043>
- Reichmann ME, Rice SA, Thomas CA, Doty P (1954) A further examination of the molecular weight and size of desoxyribose nucleic acid. *J Am Chem Soc* 76:3047–3053. <https://doi.org/10.1021/ja01640a017>
- Ruiz MC, Kljun J, Turel I, Di Virgilio AL, León IE (2019) Comparative antitumor studies of organoruthenium complexes with 8-hydroxyquinolines on 2D and 3D cell models of bone, lung and breast cancer. *Metallomics* 11:666–675. <https://doi.org/10.1039/c8mt00369f>
- Ruuskanen O, Lahti E, Jennings LC, Murdoch DR (2011) Viral Pneumonia. *Lancet* 377:1264–1275. [https://doi.org/10.1016/S0140-6736\(10\)61459-6](https://doi.org/10.1016/S0140-6736(10)61459-6)
- Sambrook J, Fritsch EF, Maniatis T (1989) Molecular cloning a laboratory manual, 2nd edn. Cold Spring Harbor Laboratory Press, Cold Spring Harbor
- Sherman SE, Lippard S (1987) Structural aspects of platinum anticancer drug interactions with DNA. *J. Chem Rev* 87:1153–1181. <https://doi.org/10.1021/cr00081a013>
- Sherman SE, Gibson D, Wang AHJ, Lippard SJ (1988) Crystal and molecular structure of cis-[Pt(NH<sub>3</sub>)<sub>2</sub>[d(pGpG)]], the principal adduct formed by cis-diamminedichloroplatinum (II) with DNA. *J Am Chem Soc* 110:7368–7381. <https://doi.org/10.1021/ja00230a017>
- Shi Y, Guo C, Sun Y, Liu Z, Xu F, Zhang Y, Wen Z, Li Z (2011) Interaction between DNA and microcystin-LR studied by spectra analysis and atomic force microscopy. *Biomacromol* 12:797–803. <https://doi.org/10.1021/bm101414w>
- Spillane CB, Smith JA, Morgan JL, Keene FR (2007) DNA affinity binding studies using a fluorescent dye displacement technique: the dichotomy of the binding site. *J Biol Inorg Chem* 12:819–824. <https://doi.org/10.1007/s00775-007-0235-9>
- Strekowski L, Wilson B (2007) Noncovalent interactions with DNA: an overview. *Mutat Res* 623:3–13. <https://doi.org/10.1016/j.mrfmmm.2007.03.008>
- Suh J, Chei WS (2008) Metallotherapeutics—novel strategies in drug design. *Curr Opin Chem Biol* 12:207–213. <https://doi.org/10.1002/chem.200900821>
- Szekely J, Gates KS (2006) Noncovalent DNA binding and the mechanism of oxidative DNA damage by fecapentaene-12. *Chem Res Toxicol* 19:117–121. <https://doi.org/10.1021/tx050197e>
- Tian F-F, Jiang F-L, Han X-L, Xiang C, Ge Y-S, Li J-H, Zhang Y, Li R, Ding X-L, Liu Yi (2010) Synthesis of a novel hydrazone derivative and biophysical studies of its interactions with bovine serum albumin by spectroscopic, electrochemical, and molecular docking methods. *J Phys Chem B* 114:14842–14853. <https://doi.org/10.1021/jp105766n>
- Timerbaev AR, Hartinger CG, Aleksenko SS, Keppler BK (2006) Interactions of antitumor metallodrugs with serum proteins: advances in characterization using modern analytical methodology. *Chem Rev* 106:2224–2248. <https://doi.org/10.1021/cr040704h>
- Vijayalakshmi R, Kanthimathi M, Subramanian V, Unni Nair B (2000) DNA cleavage by a chromium(III) complex biochem. *Biophys Res Commun* 271:731–734. <https://doi.org/10.1006/bbrc.2000.2707>

WHO site (2020). <https://www.who.int/publications/i/item/9789240015791>. Accessed 15 June 2022

Vujčić Miroslava T, Tufegdžić S, Novaković I, Djikanović D, Gašić MJ, Sladić D (2013) Studies on the interactions of bioactive quinone avarone and its methylamino derivatives with calf thymus DNA. *Int J Biol Macromol* 62:405–410. <https://doi.org/10.1016/j.ijbiomac.2013.09.013>

Zeng L, Gupta P, Chen Y, Wang E, Ji L, Chao H, Chen ZS (2017) The development of anticancer ruthenium(II) complexes: from single molecule compounds to

nanomaterials. *Chem Soc Rev* 46:5771–5804. <https://doi.org/10.1039/C7CS00195A>

**Publisher's Note** Springer Nature remains neutral with regard to jurisdictional claims in published maps and institutional affiliations.